Monte Carlo Study of Gay–Berne Liquid-crystal Droplets

Andrew P. J. Emerson† and Claudio Zannoni*
Dipartimento di Chimica Fisica ed Inorganica, Università, Viale Risorgimento,4, 40136 Bologna, Italy

We report results of a series of NVT Monte Carol simulations on systems of molecules interacting *via* a Gay–Berne (GB) potential within a spherical cavity modelling a polymer-dispersed liquid-crystal (PDLC) droplet. The cavity walls have been simulated by constructing a spherical shell of GB particles, each oriented towards the centre of the drop in an attempt to promote radial boundary conditions. The wall–fluid interactions have been modelled with a modified 1–3 GB potential (with energy exponents μ-1 and $\nu = 3$, respectively) to favour radial alignment. We show results for the molecular organization in the droplet for a 2–1 and 1–3 fluid–fluid potential. We also show the radial order parameter as a function of temperature and droplet size. It is found that at low scaled temperatures a layer of radially aligned particles is formed, but this ordering does not propagate towards the centre of the drop unless the drop is relatively large or all the fluid–fluid interactions are modelled with the 1–3 potential. In this situation, concentric shells of aligned particles are formed, with a small smectic-like domain in the centre.

1. Introduction

We describe the results of a series of NVT Monte Carlo simulations on a system of molecules interacting *via* the GB potential enclosed in a spherical cavity. The aim of these studies was to construct a model to investigate the behaviour of an extremely interesting class of materials consisting of dispersions of liquid crystals in a polymer matrix.[1] These polymer-dispersed liquid crystals (PDLC) are currently attracting considerable attention because of their electro-optic display applications.[2–8] In addition to their commercial value, PDLC are also of fundamental interest regarding the behaviour of liquid crystals in confined environments.[9] For example, a boundary-layer transition has been known to occur many degrees above the clearing point and the nematic–isotropic transition can become continuous below a critical size.[10–12] Owing to the large surface to volume ratio, surface effects dominate the observed director field. In practice, the orientation of the nematic at the droplet boundary can be controlled with suitable choices of polymer, liquid crystal and preparation conditions. For example, radial, toroidal and bipolar boundary conditions have been demonstrated.[4,6,13] These systems are of particular interest for computer simulation because the droplets can be made sufficiently small such that they contain only a few thousand molecules; this is close to the number of particles normally studied in simulations. Previous simulations of model liquid-crystal droplets have concentrated on lattice models.[14–17] They have studied, in some detail, particles interacting with the Lebwohl–Lasher potential[18] subject to various boundary conditions and to external fields and have observed many features typical of PDLC systems. However, the particles in the Lebwohl–Lasher model are constrained to a cubic lattice and so no information can be obtained on the centre-of-mass distribution. A more realistic potential for mesogenic molecules has been developed by Gay and Berne from the Gaussian overlap potential.[19] Particles interacting *via* this potential have been shown to exhibit a range of mesophases including nematic and smectic phases.[20–24] We shall now demonstrate how the GB potential can be used to investigate the molecular organization in liquid-crystal droplets by Monte Carlo simulation. We shall use a well formed from GB particles without the need for introducing the artefact, for the sizes involved, of a continuum surface.

2. The Model

2.1 GB Potential

The pair potential proposed by Gay and Berne[19] can be written as

$$U(\hat{\boldsymbol{u}}_1, \hat{\boldsymbol{u}}_2, \boldsymbol{r}) = 4\varepsilon(\hat{\boldsymbol{u}}_1, \hat{\boldsymbol{u}}_2, \hat{\boldsymbol{r}})\left\{\left[\frac{\sigma_s}{r - \sigma(\hat{\boldsymbol{u}}_1, \hat{\boldsymbol{u}}_2, \hat{\boldsymbol{r}}) + \sigma_s}\right]^{12} - \left[\frac{\sigma_s}{r - \sigma(\hat{\boldsymbol{u}}_1, \hat{\boldsymbol{u}}_2, \hat{\boldsymbol{r}}) + \sigma_s}\right]^{6}\right\} \quad (1)$$

where $\hat{\boldsymbol{u}}_1$, $\hat{\boldsymbol{u}}_2$ and $\hat{\boldsymbol{r}}$ are unit vectors defining the orientation of the two particles and of the intermolecular vector. The orientation-dependent range parameter, σ, is given by

$$\sigma(\hat{\boldsymbol{u}}_1, \hat{\boldsymbol{u}}_2, \hat{\boldsymbol{r}}) = \sigma_s\left\{1 - \frac{\chi}{2}\left[\frac{(\hat{\boldsymbol{u}}_1 \cdot \hat{\boldsymbol{r}} + \hat{\boldsymbol{u}}_2 \cdot \hat{\boldsymbol{r}})^2}{1 + \chi(\hat{\boldsymbol{u}}_1 \cdot \hat{\boldsymbol{u}}_2)} + \frac{(\hat{\boldsymbol{u}}_1 \cdot \hat{\boldsymbol{r}} - \hat{\boldsymbol{u}}_2 \cdot \hat{\boldsymbol{r}})^2}{1 - \chi(\hat{\boldsymbol{u}}_1 \cdot \hat{\boldsymbol{u}}_2)}\right]\right\}^{-1/2} \quad (2)$$

The parameter χ is determined solely by the shape anisotropy of the molecules and is

$$\chi = \frac{(\sigma_e/\sigma_s)^2 - 1}{(\sigma_e/\sigma_s)^2 + 1} \quad (3)$$

σ_e is the separation at which the attractive and repulsive terms in the potential cancel when the molecules are in the end-to-end configuration and σ_s when they are side-by-side. The energy parameter ε is defined as

$$\varepsilon(\hat{\boldsymbol{u}}_1, \hat{\boldsymbol{u}}_2, \hat{\boldsymbol{r}}) = \varepsilon_0 \varepsilon^{\nu}(\hat{\boldsymbol{u}}_1, \hat{\boldsymbol{u}}_2)\varepsilon'^{\mu}(\hat{\boldsymbol{u}}_1, \hat{\boldsymbol{u}}_2, \hat{\boldsymbol{r}}) \quad (4)$$

where

$$\varepsilon(\hat{\boldsymbol{u}}_1, \hat{\boldsymbol{u}}_2) = [1 - \chi^2(\hat{\boldsymbol{u}}_1 \cdot \hat{\boldsymbol{u}}_2)^2]^{-1/2} \quad (5)$$

and

$$\varepsilon'(\hat{\boldsymbol{u}}_1, \hat{\boldsymbol{u}}_2, \hat{\boldsymbol{r}}) = 1 - \frac{\chi'}{2}\left[\frac{(\hat{\boldsymbol{u}}_1 \cdot \hat{\boldsymbol{r}} + \hat{\boldsymbol{u}}_2 \cdot \hat{\boldsymbol{r}})^2}{1 + \chi'(\hat{\boldsymbol{u}}_1 \cdot \hat{\boldsymbol{u}}_2)} + \frac{(\hat{\boldsymbol{u}}_1 \cdot \hat{\boldsymbol{r}} - \hat{\boldsymbol{u}}_2 \cdot \hat{\boldsymbol{r}})^2}{1 - \chi'(\hat{\boldsymbol{u}}_1 \cdot \hat{\boldsymbol{u}}_2)}\right] \quad (6)$$

† Present Address: Department of Chemistry, University of Southampton, Hampshire, UK SO17 1BJ

The parameter χ' reflects the anisotropy in the attractive forces and is

$$\chi' = \frac{1 - (\varepsilon_e/\varepsilon_s)^{1/\mu}}{1 + (\varepsilon_e/\varepsilon_s)^{1/\mu}} \quad (7)$$

where ε_e and ε_s are the well-depths for the end-to-end and side-by-side configurations. Four parameters are required in order to fully specify the potential: the shape and well-depth anisotropies, σ_e/σ_s and $\varepsilon_e/\varepsilon_s$, and the energy exponents, μ and ν. The majority of simulations reported have used the values originally determined by Gay and Berne from a fit of the potential to that resulting from a line of four equidistant Lennard-Jones centres.[19] These are $\sigma_e/\sigma_s = 3$, $\varepsilon_e/\varepsilon_s = 1/5$, $\mu = 2$ and $\nu = 1$. However, this is not a unique set of parameters and other choices have also resulted in liquid-crystal phases.[20,21] The values of μ and ν are of particular interest because, as was noticed by Luckhurst *et al.*[20], for a GB particle with given shape and well-depth anisotropies the potential can be tuned to favour certain configurations. In particular, setting μ equal to 1 and ν equal to 3 stabilizes the end-to-end arrangement with respect to the perpendicular (or 'T') configuration.[21] It is this feature of the modified potential that we have found essential in our droplet simulations to model radial boundary conditions. Therefore, in this work we have employed both the 2–1 and 1–3 parametrizations for the fluid–fluid energy calculations but we have used this modified potential for the fluid–surface interactions. We shall now describe the system in more detail.

2.2 Surface Wall

The initial positional and orientational coordinates for the fluid particles in the droplet were taken from a spherical region within a previously well equilibrated Monte Carlo NVT simulation, subject to the usual cubic periodic boundary conditions. The density and temperature of this original simulation were chosen such that the system was in the isotropic phase. The centre of mass coordinates were then scaled such that they were contained in a sphere with the required radius r_d^*. It was decided to represent the polymer cavity by a spherical shell of GB particles with fixed orientations and positions. Since, in the first instance, we desired a surface which could mimic radial boundary conditions, the molecules in the shell were oriented with their symmetry axes directed towards the centre of the droplet. The positional coordinates were obtained by taking a simple cubic lattice and considering only those points which lay within a certain distance r_s^* from its centre. The value of r_s^* was chosen to be $r_d^* + 1.5$ which, for molecules with $\sigma_e/\sigma_s = 3$, prevents initial overlaps of the shell and fluid particles. Then, all but the outer shell of particles were discarded and the coordinates of the remainder scaled to lie on the surface of a sphere with radius r_s^*. In this manner an isotropic environment is created. The number of particles in the shell can be controlled by a suitable choice of lattice spacing. For the two sizes of droplet studied in detail, *i.e.* those with $r_d^* = 7.1$ and 10.0, 962 and 2018 shell particles, respectively, were found to be sufficient to prevent fluid molecules 'leaking' from the cavity. Note that, by using only one layer of these particles, we are neglecting interactions that could extend beyond the droplet walls. However, these contributions would be small and do not justify the inclusion of an additional shell which would considerably increase the computer time required.

2.3 Fluid–Wall Potential

Some earlier studies of GB droplets have suggested that simply a spherical enclosure of particles, aligned along radii of the drop, is generally insufficient to create an environment which mimics radial boundary conditions.[22] It is found that, as the scaled temperature is lowered, small smectic-like domains appear, often arranged parallel to the droplet walls. This is perhaps not surprising since systems with the GB model are known to form smectic phases readily.[23] It was therefore decided to modify the surface–fluid potential by changing the values for the energy exponents μ and ν to $\mu = 1$ and $\nu = 3$, as described earlier. The aim was to enhance the end-to-end interaction between a wall particle and a fluid particle aligned along a radius. Some preliminary simulations suggested an increased predominance of radially ordered particles and so the modified potential was adopted for the wall–fluid potential.

3. Simulation and Results

Monte Carlo simulations in the canonical ensemble (NVT) were mostly performed on two sizes of droplets: the smaller with radius $r_d^* = 7.1$ and the number of fluid particles, N_f, equal to 445; the larger with $r_d^* = 10.0$ and $N_f = 1093$. For these systems the scaled number density, ρ^* ($\rho^* = N_f \sigma_s^3/\frac{4}{3}\pi r_d^{*3}$) is equal to *ca.* 0.30, a density at which isotropic, nematic, and smectic-B phases have been observed in bulk phase simulations.[23] The usual 2–1 GB potential was used to model the interactions between fluid particles while the 1–3 potential was employed for the wall–fluid interactions. Simulations were also attempted on a droplet containing *ca.* 10^4 particles, but the excessive computation necessary meant that only a few temperatures could be studied so we shall not report these in detail. In order to examine the situation where the fluid–fluid coupling is the same as that for the wall–fluid one, a further set of simulations for the $r_d^* = 10$ droplet were performed with both sets of interactions modelled by the 1–3 potential. During a run, trial orientations were generated with the Barker–Watts technique[24] and the maximum angular and translational displacements adjusted to give an acceptance ratio of *ca.* 0.5. A cut-off of the potential of $4.0\sigma_s$ and a Verlet neighbour list with a list radius of $4.8\sigma_s$ were employed to reduce the computer time required.[25]

Simulations were performed as a function of scaled temperature, T^* ($T^* = KT/\varepsilon_0$), each run being started from a configuration at a higher temperature. Typically (40–50) $\times 10^3$ cycles (where 1 cycle $\equiv N_f$ attempted moves) were employed for equilibration and *ca.* 20×10^3 cycles for production. The apparent absence of first-order phase transitions did not demand the prolonged equilibrations often required for GB simulations in the bulk.[21] The orientational ordering was monitored during the simulations from the value of $\langle P_2 \rangle$, determined in the usual way from diagonalization of the molecular Q tensor.[26,27] The degree of radial ordering in the system was estimated from a second-rank radial order parameter, $\langle P_2 \rangle_r$, first introduced by Chiccoli *et al.*,[14]

$$\langle P_2 \rangle_r = \frac{1}{N_f} \left\langle \sum_{i=1}^{N_f} P_2(\boldsymbol{u}_i \cdot \boldsymbol{r}_i) \right\rangle \quad (8)$$

where $\boldsymbol{u}_i$ is the direction cosine of the ith particle and $\boldsymbol{r}_i$ is its radial vector. Thus $\langle P_2 \rangle_r$ is equal to unity for a perfectly ordered 'hedgehog' configuration, and close to zero for a randomly oriented system. Notice that $\langle P_2 \rangle_r$ will become negative if at a given distance r the molecules are on average forming an angle greater than the magic angle with the radial direction. The average values of the scaled internal energy per particle, $U^*(U^* = U/N\varepsilon_0)$, $\langle P_2 \rangle$ and $\langle P_2 \rangle_r$ obtained from the simulations are listed in Tables 1–3. The errors in the averages were estimated by dividing each run into smaller runs of *ca.* 1000 cycles in length, as described in ref. 28. We report in

Table 1 Average energies and radial order parameters for the droplet with $r_d^* = 7.1$ and $N_f = 445$

T^*	$\langle E \rangle$	$\langle P_2 \rangle_r$
0.4	−7.931 ± 0.009	0.679 ± 0.001
0.6	−7.408 ± 0.007	0.708 ± 0.002
0.7	−7.082 ± 0.008	0.680 ± 0.002
0.8	−6.781 ± 0.010	0.661 ± 0.005
1.0	−6.205 ± 0.018	0.622 ± 0.005
1.1	−5.856 ± 0.017	0.596 ± 0.004
1.2	−5.568 ± 0.018	0.574 ± 0.004
1.3	−5.373 ± 0.015	0.552 ± 0.003
1.4	−5.176 ± 0.020	0.575 ± 0.002
1.5	−4.695 ± 0.009	0.502 ± 0.002
1.6	−4.269 ± 0.011	0.442 ± 0.005
1.7	−4.134 ± 0.009	0.447 ± 0.005
1.8	−3.791 ± 0.011	0.388 ± 0.003
1.9	−3.568 ± 0.015	0.348 ± 0.005
2.0	−3.299 ± 0.017	0.316 ± 0.005
2.5	−2.069 ± 0.021	0.150 ± 0.006
3.0	−1.305 ± 0.014	0.071 ± 0.005

Table 2 Average energies and radial order parameters for the droplet with $r_d^* = 10.0$ and $N_f = 1093$

T^*	$\langle E \rangle$	$\langle P_2 \rangle_r$
0.4	−7.151 ± 0.002	0.629 ± 0.002
0.6	−6.469 ± 0.004	0.615 ± 0.001
0.8	−5.896 ± 0.006	0.594 ± 0.001
1.0	−5.294 ± 0.009	0.535 ± 0.002
1.2	−4.681 ± 0.004	0.471 ± 0.002
1.4	−3.989 ± 0.007	0.381 ± 0.003
1.6	−3.320 ± 0.005	0.241 ± 0.002
1.8	−2.911 ± 0.006	0.182 ± 0.002
2.0	−2.590 ± 0.007	0.124 ± 0.002
2.2	−2.294 ± 0.004	0.089 ± 0.003
2.4	−2.092 ± 0.005	0.074 ± 0.002
2.6	−1.868 ± 0.003	0.056 ± 0.002
2.8	−1.675 ± 0.004	0.038 ± 0.001
3.0	−1.491 ± 0.004	0.029 ± 0.002

Table 3 Average energies and radial order parameters for the droplet with $r_d^* = 10.0$ and $N_f = 1093$ and with the 1–3 potential for fluid–fluid interactions

T^*	$\langle E \rangle$	$\langle P_2 \rangle_r$
1.0	−13.005 ± 0.022	0.887 ± 0.001
1.2	−12.372 ± 0.007	0.888 ± 0.001
1.4	−11.740 ± 0.010	0.867 ± 0.001
1.6	−11.092 ± 0.009	0.836 ± 0.001
1.7	−10.756 ± 0.010	0.812 ± 0.002
1.8	−10.340 ± 0.009	0.796 ± 0.001
2.0	−9.594 ± 0.015	0.735 ± 0.001
2.2	−8.593 ± 0.019	0.702 ± 0.005
2.3	−8.236 ± 0.016	0.696 ± 0.002
2.4	−7.478 ± 0.024	0.615 ± 0.003
2.5	−7.178 ± 0.040	0.592 ± 0.005
2.6	−6.440 ± 0.012	0.415 ± 0.003
2.8	−5.305 ± 0.022	0.327 ± 0.007
3.0	−4.123 ± 0.019	0.161 ± 0.005
3.2	−3.611 ± 0.020	0.081 ± 0.006

detail the results for the droplet cavity with fluid particles interacting *via* the 2–1 GB potential and then briefly some results for the modified 1–3 potential.

3.1 2–1 GB fluid

In Fig. 1 we show the average value of the second-rank orientational order parameter, $\langle P_2 \rangle$, as a function of scaled tem-

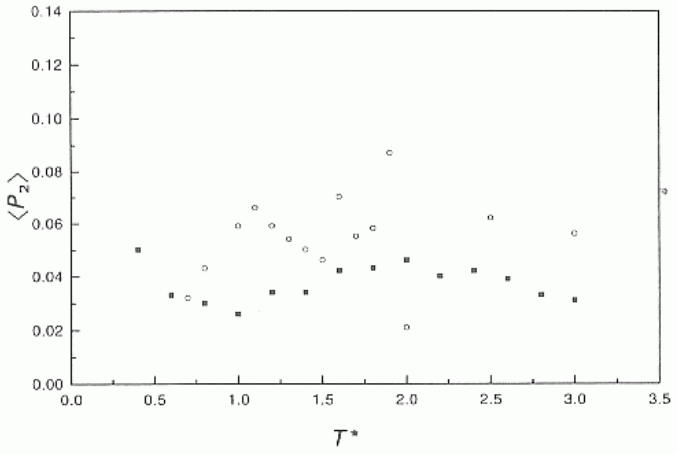

Fig. 1 Variation of second-rank order parameter, $\langle P_2 \rangle$, with scaled temperature for $r_d^* = 7.1$ (○) and 10.0 (■)

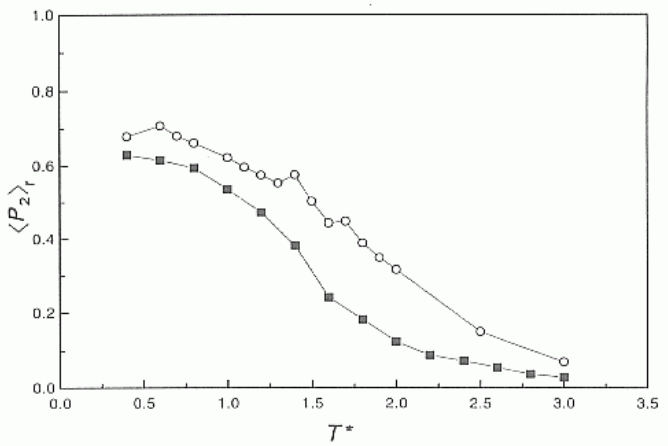

Fig. 2 $\langle P_2 \rangle_r$, as a function of scaled temperature for $r_d^* = 7.1$ (○) and 10.0 (■)

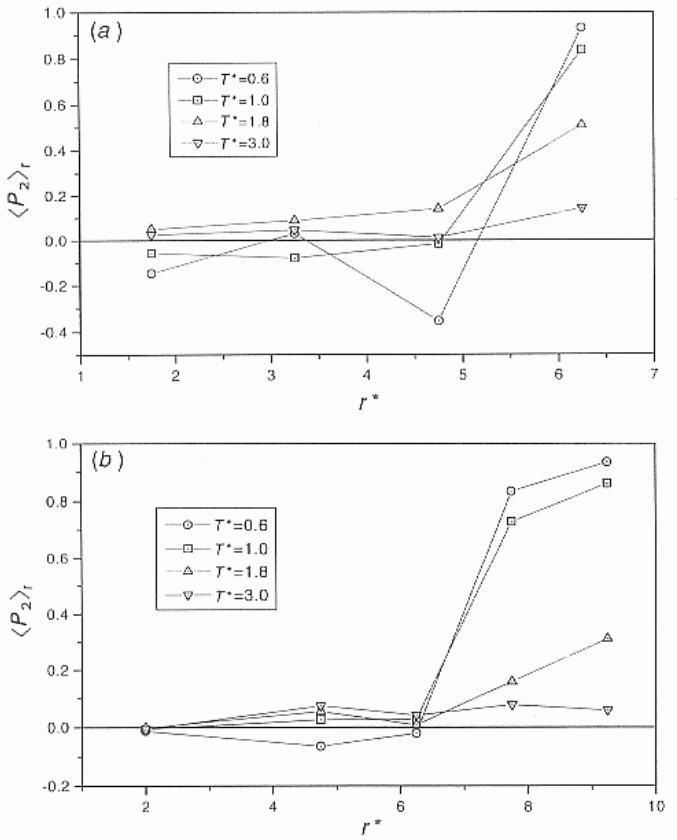

Fig. 3 $\langle P_2 \rangle_r$ as a function of scaled distance from the centre of the drop, r^*, for drops with $r_d^* = (a)$ 7.1 and (b) 10.0 and for the four scaled temperatures indicated

perature for both droplet sizes. We see that at every temperature $\langle P_2 \rangle$ never rises above *ca.* 0.1, indicating that the system is always isotropic; the order parameter is not exactly zero because of the statistical uncertainty, of the order of $O(N_f^{-1/2})$, in evaluating $\langle P_2 \rangle$ from the Q tensor.[29] This is in contrast to the bulk system where a nematic–isotropic transition is observed at $T^* \approx 0.9$ at this density.[23] The variation of the second-rank radial order parameter, $\langle P_2 \rangle_r$, with scaled temperature is shown in Fig. 2. For both system sizes there is a gradual increase in radial order as the temperature is lowed but it reaches a maximum value of $\langle P_2 \rangle_r = 0.6$–$0.7$. Thus, even at the lowest temperatures simulated, the radial ordering is not complete. The origin of this maximum can be inferred from the variation of $\langle P_2 \rangle_r$ with r^* within the drop. In Fig. 3(*a*) we show the radial order parameters calculated from the particles contained in four concentric shells in the smaller drop; Fig. 3(*b*) shows, the order parameters for five regions in the larger drop. We see from both plots that the radial order is very high near the edge of the drop with $\langle P_2 \rangle_r$ approaching unity at the lower temperatures. However, when we move more than one molecular length (1 molecular length $\equiv 3\sigma_s$) away from the walls, the order parameter rapidly drops to zero or even negative values. It is observed that $\langle P_2 \rangle_r$ is closer to zero in the larger drop in these regions, probably because of the better statistics with the greater number of particles. From this data we can deduce that radial order is the highest nearest the walls of the drop and is almost perfect at the lower temperatures, while in the centre of the drop it is relatively disordered at all temperatures.

In Fig. 4 we show the density profile, $\rho^*(r^*)$, as a function of distance r^* from the centre of the drop at four temperatures for both drop sizes. The distributions have been normalised such that for a homogeneous fluid $\rho^*(r^*) = 1$. In each plot we see that a single peak forms near the drop wall which is consistent with the formation of a radially aligned layer. At all other distances, however, $\rho^*(r^*)$ is essentially unity. Note also that, since the peaks occur at about $r_d^* - 1$ and the particles are 3 scaled units in length, then there has been some adsorption on the wall surface.

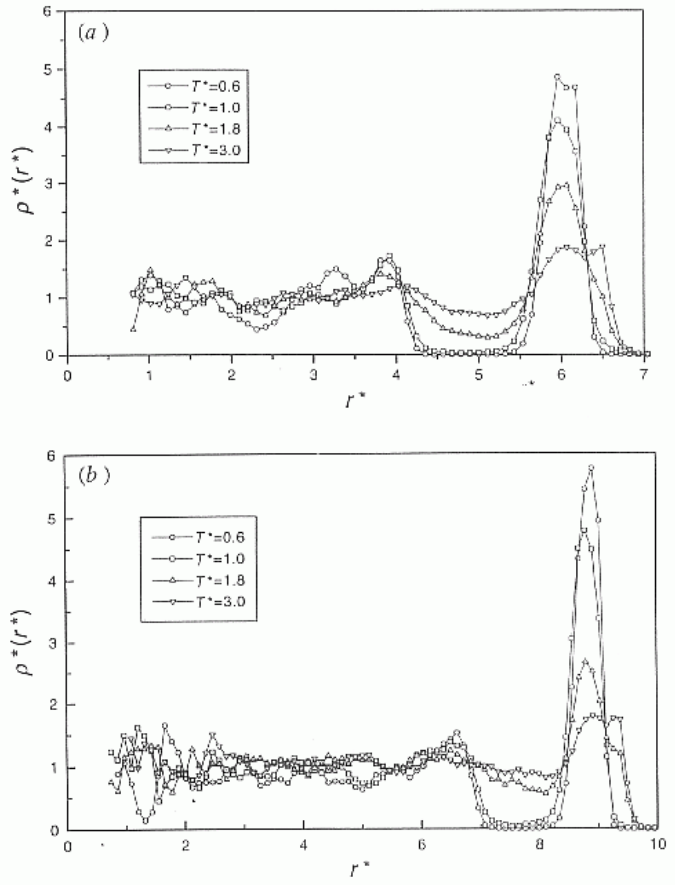

Fig. 4 Density distribution as a function of scaled distance, r^*, from the centre of the drop with $r_d^* =$ (*a*) 7.1 and (*b*) 10.0 and for four scaled temperatures

The molecular organization within the droplets can be readily discerned from 'snap-shots' of some sample configurations. Plate 1 shows equatorial sections of both droplets at a high temperature ($T^* = 3.0$) and at a low temperature ($T^* = 0.6$) The particles are depicted as ellipsoids whose sizes are in correct proportion to the dimensions of the droplet and colour coded to represent their orientations.[21] Also included are snapshots from simulations of a larger droplet with $r_d^* = 20$ and with $N_f \sim 10^4$ particles. Let us first consider the two smaller drops shown in Plate 1(*a*) and (*b*). At $T^* = 3.0$ the particles are essentially randomly located and oriented within the drop. At the much lower temperature of 0.6, it is evident in both systems that a layer of radially aligned particles has formed on the wall surface. However, this radical order has not propagated towards the centre. Instead we observe that small smectic-like domains have formed. This explains why $\langle P_2 \rangle_r$ only reaches of maximum of *ca.* 0.6 since only a proportion of the particles are oriented towards the centre. On lowering the temperature from the isotropic phase, $\langle P_2 \rangle_r$ rises as the boundary layer is formed. However, once the layer is complete, $\langle P_2 \rangle_r$ remains constant since no further particles align along a radius. It would appear that for this GB system the presence of a first shell of radially oriented molecules does not initiate further alignment towards the centre of the droplet. We note that this is different to the model droplet of Chiccoli *et al.* with the Lebwohl–Lasher potential where, for instance with inside–outside coupling equal to that between the droplet molecules, at low temperatures virtually all the particles are pointing towards the centre and the value of $\langle P_2 \rangle_r$ is close to unity.[14,15] The behaviour observed here is also at variance with the existence of a hedgehog defect expected from continuum theory.[9] The situation is different for the much larger drop [Plate 1(*c*)]. Here, starting from a disordered configuration it is observed that further shells have formed. For this system size, the molecules behave more like those present in a bulk fluid and so they form a phase which is reminiscent of those found in smectics.

3.2 1–3 GB fluid

For these simulations the fluid–fluid coupling has the same characteristics as that between the fluid and wall. Fig. 5 shows the variation of $\langle P_2 \rangle_r$ with scaled temperature. Again we see a gradual rise as the temperature is lowered but this time the maximum value of $\langle P_2 \rangle_r$ is much higher, *ca.* 0.9. This suggests that many more molecules are radially ordered. In addition, it can be noticed that $\langle P_2 \rangle_r$ rises more rapidly with temperature than for the simulations with the 2–1 potential. Snapshots of some configurations at three scaled temperatures are shown in Plate 2. In a similar fashion to that observed for the system with the 2–1 GB potential, a layer of molecules forms at the droplet walls but at lower temperatures we also observe two other concentric shells of particles. It would appear then that as a result of the enhanced end-to-end attraction with the modified potential the formation of the first shell can induce other ones, at low temperatures. For this size of droplet, $r_d^* = 10$, there is essentially only space for three shells of particles to form and so a small domain of liquid-crystal-like material forms in the centre.

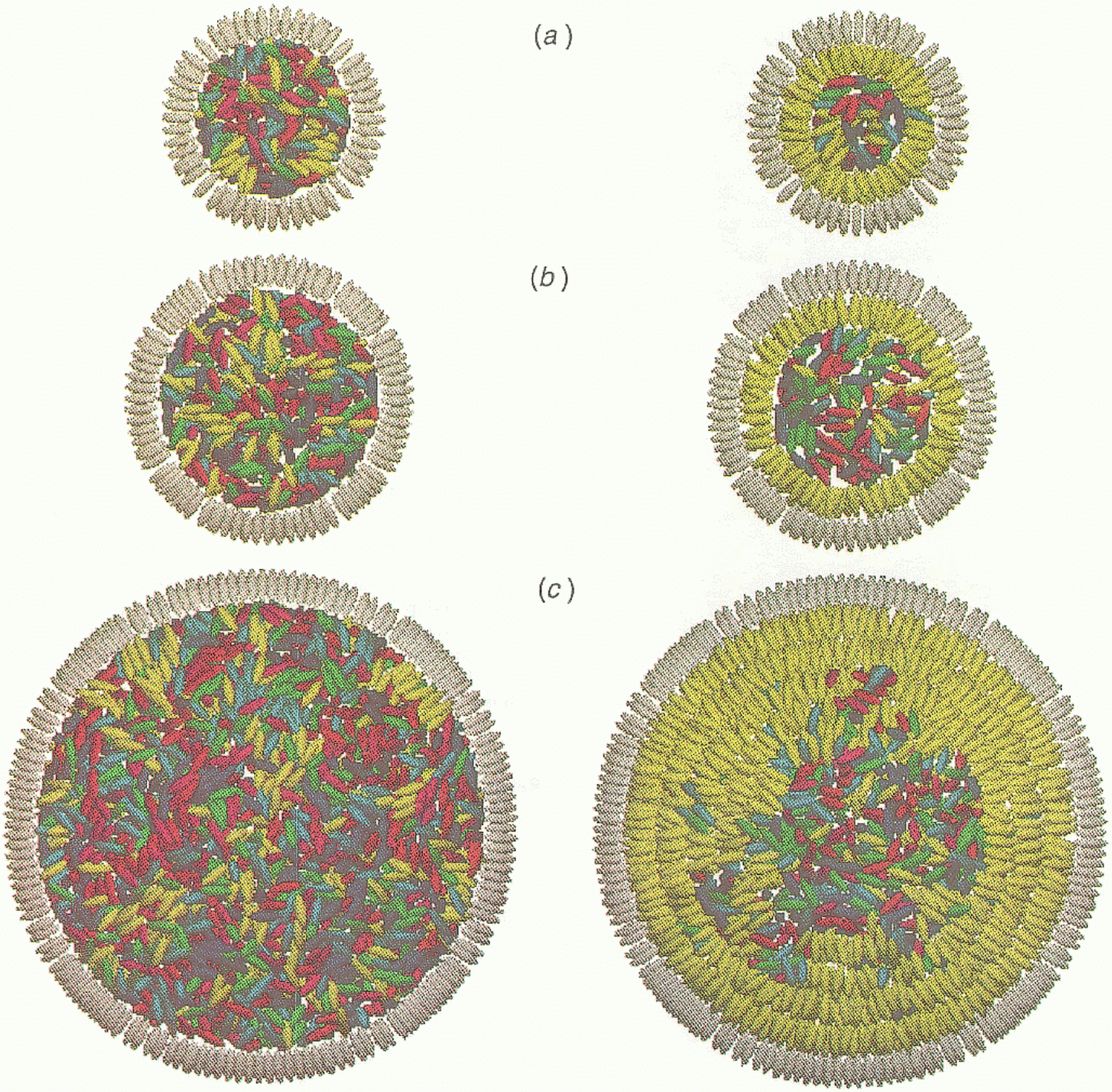

Plate 1 Snaphots of equatorial sections of the GB droplet with radii r_d^* of (*a*) 7.1, (*b*) 10.0 and (*c*) 20.0. The left-hand image shows a droplet at a scaled temperature, T^*, of 3.0 and the right-hand image one at a scaled temperature of 0.6. Each particle has been coloured according to its orientation with respect to its radial vector. For example, a particle in yellow tends to be oriented along a radius while one in blue is at right angles to it. The shell particles representing the polymer are coloured grey.

4. Conclusions

We have demonstrated how the GB model mesogen can be used to model the molecular organization present within dispersed liquid-crystal droplets subject to radial boundary conditions. It has been found necessary, to use the modified 1–3 GB potential, first studied by Berardi *et al.*[21] for the fluid–surface interactions in order to enhance the propensity for the particles to align along a radius. With this modified fluid–surface potential a shell of radially aligned particles forms close to the walls of the droplet but this order does not propagate further than this single shell except for drops with at least $r_d^* > 10$. By using the 1–3 potential for all the particle interactions, further concentric shells of radially aligned particles are induced at sufficiently low scaled temperatures for $r_d^* = 10.0$. These results could be described at least as partially realistic in so far as we have demonstrated the suppression of the nematic–isotropic transition, as is often observed experimentally in small droplets, and the competition between droplet curvature and the elastic forces that stabilize the usual bulk liquid-crystal phases. At the low temperature employed, the local ordering in the simulated droplets is smectic-like, rather than the more often observed nematic-PDLC. Perhaps the problem here is the propensity for particles interacting through the standard 2–1 GB potential to form smectic phases; the phase diagram of de Miguel *et al.* predicts that nematics only appear over a relatively limited range of densities and temperatures.[23] This is exemplified by our observation that the boundary conditions, designed to be radial in a similar way to the droplet simulations based on the Lebwohl–Lasher potential, are insufficient to induce

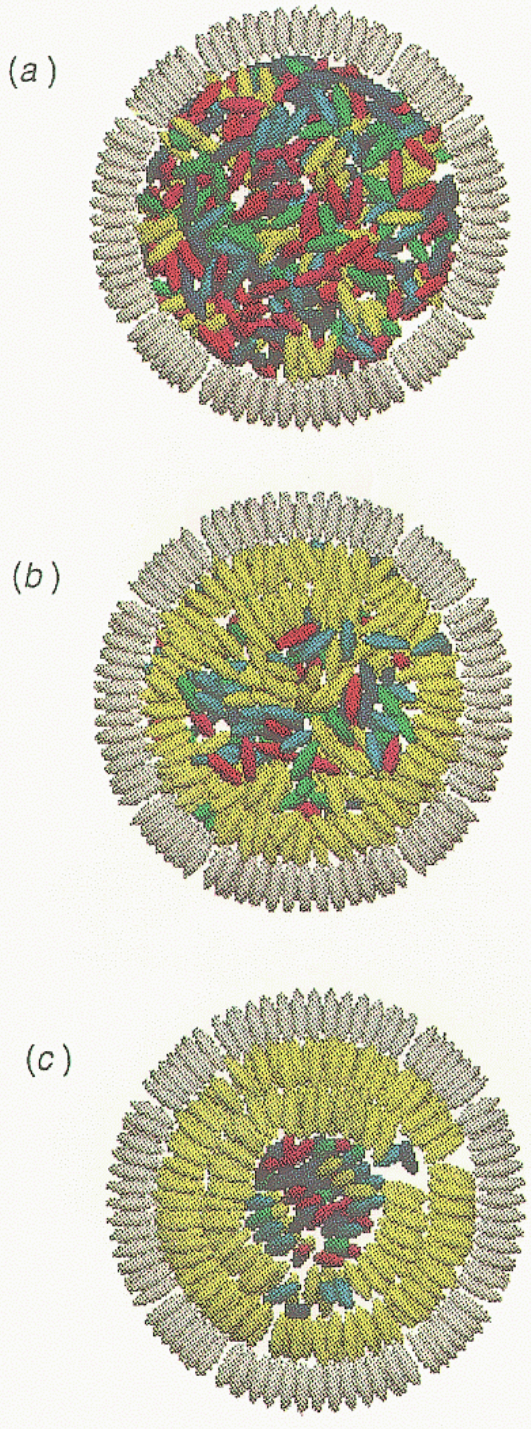

Plate 2 Snapshots of equatorial sections of the droplet with $r_d^* = 10.0$ and with the 1–3 GB potential for the fluid–fluid interactions at: (*a*) 4.0 (*b*) 2.5 and (*c*) 1.0. The particles are coloured as in Plate 1.

radial ordering at temperatures high enough to prevent the particles packing closely together. For a more accurate representation of the situation within PDLC it might also be necessary to use larger system sizes. With a rough calculation, based on 4-*n*-pentyl-4'-cyanobiphenyl (5CB), our largest droplet ($N_t \sim 10^4$ particles) corresponds to a cavity size with a diameter less than *ca.* 0.01 μm, similar in size to the smallest droplet size studied,[11] even though, most often, droplets in PDLC systems tend to have diameters of *ca.* 2–3 μm.[2] However, with the ever increasing availability of high-performance computer systems simulations with 10, or even 100, times the number of particles reported in this article are becoming perfectly feasible.

Thus computer simulations offer a fascinating possibility of obtaining the molecular organization inside these materials

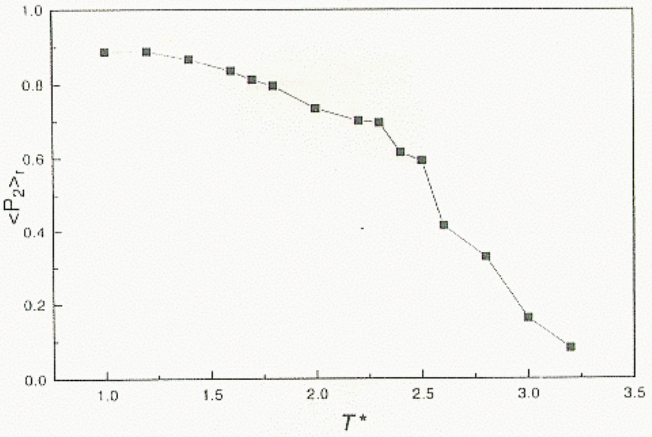

Fig. 5 $\langle P_2 \rangle_r$ as a function of scaled temperature for the drop with $r_d^* = 10.0$ and with the fluid–fluid interactions modelled using the 1–3 GB potential

dominated by surface effects as well as the changes induced by variations in the anchoring strength or more generally in the wall–particle potential.

We are grateful to the Royal Society (London) for a postdoctoral fellowship for A.E., to MURST, CNR and the EU, H.C.M. programme for support and to CINECA (Icarus project) for Cray T3D time. We also wish to thank C. Chiccoli, P. Pasini, S. Roskilly and F. Semeria for help and discussions.

References

1 G. P. Crawford and J. W. Doane, *Condens. Matter News*, 1992, **1**, 5.
2 J. W. Doane, in *Liquid Crystals—Applications and Uses*, ed. B. Bahadur, World Scientific Publishing, 1990, vol. 1, p 361.
3 J. W. Doane, *MRS Bulletin*, 1991, 22.
4 H. S. Kitzerow, *Liq. Cryst.*, 1994, **16**, 1.
5 P. S. Drzaic, *J. Appl. Phys.*, 1986, **60**, 2142.
6 G. Spruce and R. D. Pringle, *Electron. Commun. Eng. J.*, 1992, **4**, 91.
7 K. Kato, K. Tanaka, S. Tsuru and S. Sakai, *Jpn. J. Appl. Phys. 1*, 1993, **32**, 4594.
8 C. M. Lampert, *Thin Solid Films*, 1993, **236**, 6.
9 (*a*) N. Schopohl and T. J. Sluckin, *J. Phys.*, 1988, **49**, 1097; (*b*) C. Chiccoli, P. Pasini, F. Semeria, T. J. Sluckin and C. Zannoni, *J. Phys. II*, 1995, **5**, 427.
10 A. Poniewierski and T. J. Sluckin, *Liq. Cryst.*, 1987, **2**, 281.
11 A. Golemme, S. Zumer, D. W. Allender and J. W. Doane, *Phys. Rev. Lett.*, 1988, **61**, 2937.
12 S. Kralj, S. Zumer and D. W. Allender, *Phys. Rev. A*, 1991, **43**, 2943.
13 G. Chidichimo, G. Arabia, A. Golemme and J. W. Doane, *Liq. Cryst.*, 1989, **5**, 1443.
14 C. Chiccoli, P. Pasini, F. Semeria and C. Zannoni, *Phys. Lett. A.*, 1990, **150**, 311.
15 C. Chiccoli, P. Pasini, F. Semeria and C. Zannoni, (*a*) *Mol. Cryst. Liq. Cryst.*, 1992, **212**, 197; (*b*) *Mol. Cryst. Liq. Cryst.*, 1992, **221**, 19.
16 E. Berggren, C. Zannoni, C. Chiccoli, P. Pasini and F. Semeria, (*a*) *Chem. Phys. Lett.*, 1992, **197**, 224. (*b*) *Phys. Rev. E*, 1994, **49**, 614.
17 E. Berggren, C. Zannoni, C. Chiccoli, P. Pasini, F. Semeria, *Phys. Rev. E*, 1994, **50**, 2929.
18 P. A. Lebwohl and G. Lasher, *Phys. Rev. A.*, 1972, **6**, 426.
19 J. G. Gay and B. J. Berne, *J. Chem. Phys.*, 1981, **74**, 3316.
20 R. A. Stephens, G. R. Luckhurst and R. W. Phippen, *Liq. Cryst.*, 1990, **8**, 451.
21 R. Berardi, A. P. J. Emerson and C. Zannoni, *J. Chem. Soc., Faraday Trans.*, 1993, **89**, 4069.
22 A. P. J. Emerson, C. Chiccoli, P. Pasini, F. Semeria and C. Zannoni, presented at the 14th ILCC, Pisa (H-P19), 1992.

23 E. De Miguel, L. F. Rull, M. K. Chalam and K. E. Gubbins, *Mol. Phys.*, 1991, **74**, 2, 405.
24 J. A. Barker and R. O. Watts, *Chem. Phys. Lett.*, 1969, **3**, 144.
25 M. P. Allen and D. J. Tildesley, *Computer Simulation of Liquids*, Clarendon Press, Oxford, 1987.
26 J. Viellard-Baron, *Mol. Phys.*, 1974, **28**, 809.
27 C. Zannoni, in *The Molecular Physics of Liquid Crystals*, ed. G. R. Luckhurst and G. W. Gray, Academic Press, London, 1979, ch. 9, p. 191.
28 C. Zannoni, *J. Chem. Phys.*, 1986, **84**, 1, 424.
29 R. Eppenga and D. Frenkel, *Mol. Phys.*, 1984, **52**, 1303.

Paper 5/02848E; *Received* 3*rd May*, 1995